

International Telecommunication Union

ITU-R
Radiocommunication Sector of ITU

Report ITU-R P.2297-0
(06/2013)

**Electron density models and data for
transionospheric radio propagation**

P Series
Radiowave propagation



International
Telecommunication
Union

Foreword

The role of the Radiocommunication Sector is to ensure the rational, equitable, efficient and economical use of the radio-frequency spectrum by all radiocommunication services, including satellite services, and carry out studies without limit of frequency range on the basis of which Recommendations are adopted.

The regulatory and policy functions of the Radiocommunication Sector are performed by World and Regional Radiocommunication Conferences and Radiocommunication Assemblies supported by Study Groups.

Policy on Intellectual Property Right (IPR)

ITU-R policy on IPR is described in the Common Patent Policy for ITU-T/ITU-R/ISO/IEC referenced in Annex 1 of Resolution ITU-R 1. Forms to be used for the submission of patent statements and licensing declarations by patent holders are available from <http://www.itu.int/ITU-R/go/patents/en> where the Guidelines for Implementation of the Common Patent Policy for ITU-T/ITU-R/ISO/IEC and the ITU-R patent information database can also be found.

Series of ITU-R Reports

(Also available online at <http://www.itu.int/publ/R-REP/en>)

Series	Title
BO	Satellite delivery
BR	Recording for production, archival and play-out; film for television
BS	Broadcasting service (sound)
BT	Broadcasting service (television)
F	Fixed service
M	Mobile, radiodetermination, amateur and related satellite services
P	Radiowave propagation
RA	Radio astronomy
RS	Remote sensing systems
S	Fixed-satellite service
SA	Space applications and meteorology
SF	Frequency sharing and coordination between fixed-satellite and fixed service systems
SM	Spectrum management

Note: This ITU-R Report was approved in English by the Study Group under the procedure detailed in Resolution ITU-R 1.

Electronic Publication
Geneva, 2014

© ITU 2014

All rights reserved. No part of this publication may be reproduced, by any means whatsoever, without written permission of ITU.

REPORT ITU-R P.2297-0

Electron density models and data for transionospheric radio propagation

(2013)

Scope

This Report presents the detailed characteristics of electron density and total electron content models essential to Recommendation ITU-R P.531 for transionospheric propagation and supplementary digital Vertical TEC grid point maps.

TABLE OF CONTENTS

	<i>Page</i>
1 Introduction	1
2 IRI-2012 electron density model	2
2.1 Introduction.....	2
2.2 Changes in version IRI-2012	3
2.3 References.....	4
3 NeQuick2 electron density model	6
3.1 Background.....	6
3.2 The NeQuick electron density model	6
3.3 Electron density computation	17
3.4 TEC calculation	20
3.5 Changes introduced in NeQuick2	26
3.6 References.....	28
4 Vertical Total Electron Content maps	28

1 Introduction

As reported in Recommendation ITU-R P.531, a number of transionospheric propagation effects, such as refraction, dispersion and group delay, are in magnitude directly proportional to the Total Electron Content (TEC); Faraday rotation is also approximately proportional to TEC, with the contributions from different parts of the ray path weighted by the longitudinal component of magnetic field. Knowledge of the TEC thus enables many important ionospheric effects to be estimated quantitatively.

For estimating TEC, either a procedure based on the international reference ionosphere (IRI) or a procedure based on NeQuick, is recommended in Recommendation ITU-R P.531. The latter procedure is also suitable for slant TEC evaluation. Both models are climatological electron density

models and their details are provided in the following chapters. The last chapter includes example Vertical TEC monthly mean (and standard deviation) grid maps data obtained from measurements at a set of periods and solar activities.

2 IRI-2012 electron density model

2.1 Introduction

The International Reference Ionosphere (IRI) is a joint project of the Committee on Space Research (COSPAR) and the International Union of Radio Science (URSI). The IRI Working Group, consisting of 50+ experts from different countries representing the modelling and measuring (ground and space) communities, was established to develop and improve a reference model for the most important plasma characteristics in Earth's ionosphere. The model should be primarily based on experimental evidence using all available ground and space data sources and should not depend on the evolving theoretical understanding of ionospheric processes. But theoretical considerations can help to find the appropriate mathematical functions, to bridge data gaps and for internal consistency checks. As new data become available and as older data sources are fully evaluated and exploited, the model should be revised in accordance with these new results. COSPAR's prime interest is in a general description of the ionosphere as part of the terrestrial environment for the evaluation of environmental effects on spacecraft and experiments in space. URSI's prime interest is in the electron density part of IRI for defining the background ionosphere for radiowave propagation studies and applications.

IRI describes monthly averages of electron density, electron temperature, ion temperature, and the percentage of O^+ , H^+ , He^+ , N^+ , NO^+ , O_2^+ , and Cluster ions in the altitude range from 50 km to 1500 km. In addition IRI provides the total ionospheric electron content (TEC), ion drift at the equator, occurrence probability for spread-F and F1-layer. IRI is included in the NASA-supported Community Coordinate Modelling Center (CCMC) and the Virtual Model Depository (VMD). IRI is part of ESA's European Cooperation for Space Standardization (ECCS) and it is the technical specification for the ionospheric environment recommended by the International Standardization Organization. IRI is similar to standards for other parts of the space environment like CIRA/MSIS, IGRF, etc.

The IRI model of electron density profiles is based on maps of the peak characteristic of the ionospheric layers: $foF2$, $foF1$, and foE , and the corresponding heights $hmF2$, $hmF1$, and hmE . The earliest version of the IRI model, IRI-78 (Rawer *et al.*, 1978a, 1978b) used the $foF2$ model that was developed for ITU's Comité Consultatif International des Radiocommunications (CCIR) and it is therefore commonly referred to as the CCIR $foF2$ model. The model is described in detail in ITU's CCIR Atlas of Ionospheric Characteristics (CCIR, 1966).

The model was developed by Jones and Gallet (1962) and Jones *et al.* (1969) based on global ionosonde data from the time period 1954 to 1958. In order to avoid numerical instabilities artificial values, so-called 'screen points', were introduced in areas where no measurements were available, specifically in the large ocean areas and in parts of the southern hemisphere. These screen points were determined by extrapolation along lines of constant modified dip latitude. The model describes $foF2$ in terms of geographic latitude, longitude, modified dip latitude, and UT, and consists of 24 maps of 988 coefficients each, one for each month of the year and for two levels of solar activity, $R_{12} = 10$ and 100, where R_{12} is the 12-month running-mean of the monthly sunspot number R_m ($2 \cdot 12 \cdot 988 = 23,712$ coefficients in all). Linear interpolation is recommended for intermediate times and solar activities. But because of an often observed saturation effect at high solar activities the ITU document recommends to keep R_{12} at the saturation value of 150 even when R_{12} exceeds this upper threshold value.

2.2 Changes in version IRI-2012

The newest version of the IRI model, IRI-2012, includes significant improvements not only for the representations of electron density, but also for the description of electron temperature and ion composition. These improvements are the result of modelling efforts since the last major release, IRI-2007. Modelling progress is documented in several special issues of *Advances in Space Research*: Volume 39, Number 5, 2007; Volume 42, Number 4, August 2008; Volume 43, Number 11, June 2009; Volume 44, Number 6, September 2009.

(1) In the bottomside the IRI electron density profile is normalized to the E and F2 peaks and the shape of the profile is determined by the bottomside thickness parameter B0 and the shape parameter B1. Currently two options are given for these parameters: (i) the standard option consisting of a table of values and associated interpolation scheme (Bilitza *et al.*, 2000) and (ii) the Gulyaeva option based on the model of Gulyaeva (1987) utilizing the half-density point h0.5 where the topside density has dropped down to half the peak density. Shortcomings of these older models are their limited database and the resulting misrepresentation of variations with season, latitude and solar activity. Altadill *et al.* (2008, 2009) have applied spherical harmonic analysis to data from 27 globally distributed ionosonde stations obtaining a new model for B0 and B1 that more accurately describes the observed variations with latitude, local time, month, and sunspot number. Overall the improvements over the older IRI model are of the order of 15 to 35%. The largest improvements are seen at low latitudes.

(2) At high-latitudes, the off-set of the magnetic pole from the geographic pole and its rotation around the geographic (rotation axis) pole together with the influx of energetic solar wind particles results in the formation of the auroral oval at the boundary between closed and open magnetic field lines. Ionospheric densities and temperatures exhibit characteristic variations in and near the oval region and therefore the inclusion of an oval description in IRI has long been a high priority of the IRI team (e.g. Szuszczewicz, 1993 and Bilitza, 1995) and is the first step towards including the high-latitude characteristics in IRI. Zhang and Paxton (2008) have recently developed a model of the auroral electron energy flux based on global Far Ultraviolet (FUV) measurements with the Global Ultraviolet Imager (GUVI) on the Thermosphere Ionosphere Mesosphere Energetics and Dynamics (TIMED) satellite. The model also describes the expansion of the oval during magnetic storms. Using threshold fluxes we can define the boundaries of the oval and their movement with magnetic activity (Zhang *et al.*, 2010). This boundary parameterization is included in IRI-2012.

(3) During nighttime Infrared emissions measured by another TIMED instrument, the Sounding of the Atmosphere using Broadband Emission Radiometry (SABER) instrument, will help us to represent in IRI the storm induced enhancements of the E-region electron density that is caused by increased particle precipitation. Mertens *et al.* (2007) and Fernandez *et al.* (2010) have developed a model for the E-peak enhancement for different levels of magnetic activity using a formalism similar to the one used in the F-region STROM model of Fuller-Rowell *et al.* (2000). Comparisons with incoherent scatter radar measurements show good agreement (Fernandez *et al.*, 2010). This E-region storm model is included in IRI-2012.

(4) IRI-2012 makes use of the latest version of the International Geomagnetic Reference Field (IGRF, 2010) for its computation of magnetic coordinates. With IRI-2012 the software for computing Corrected Geomagnetic Coordinates is included in the model and used for the auroral boundary specification.

(5) The Distribution of molecular ions in the bottomside ionosphere is improved in IRI-2012 based on FLIP-model photochemistry normalized to the IRI electron density (= total ion density) (Richards *et al.*, 2010). Below ~150 km, the relative ion concentrations can be determined from chemical equilibrium calculation. Above ~150 km the O⁺ density diffusion becomes important; solution: use the electron density provided by the IRI model. The iterative technique solves for O⁺ density:

$$[O+] = [e] - ([O2+] + [NO+] + [N2+] + [N+]) \quad \text{with } [e] = \text{IRI electron density}$$

O2+, NO+, N2+, N+, and NO densities determined from Production = Loss

(6) Neutral atmosphere model MSIS-86 is replaced by the newer NRL-MSIS-00 (Picone *et al.*, 2002). Densities are being used by the new bottomside ion composition model (5). Neutral temperature is used as lower boundary for electron and ion temperature.

(7) A new model for the topside electron temperature is included in IRI-2012 that includes variations with solar activity (Bilitza *et al.*, 2007; Truhlik *et al.*, 2009, 2011).

IRI2012 can be obtained from: <http://iri.gsfc.nasa.gov/>.

2.3 References

- Altadill, D., D. Arrazola, E. Blanch, and D. Buresova (2008), Solar activity variations of ionosonde measurements and modelling results. *Adv. Space Res.* 42: 610–616.
- Altadill, D., J.M. Torta, and E. Blanch (2009), Proposal of new models of the bottom-side B0 and B1 parameters for IRI. *Adv. Space Res.* 43: 1825-1834. doi:10.1016/j.asr.2008.08.0144.
- Bilitza, D. (1995), Including auroral boundaries in the IRI model. *Adv. Space Res.* 16(1): 13-16.
- Bilitza, D., International Reference Ionosphere 1990, 155 pages, National Space Science Data Center, NSSDC/WDC-A-R&S 90-22, Greenbelt, Maryland, November 1990.
- Bilitza, D., International Reference Ionosphere 2000, *Radio Science* 36, #2, 261-275, 2001.
- Bilitza, D., K. Rawer, and S. Pallaschke, Study of ionospheric models for satellite orbit determination, *Radio Science* 23, 223-232, 1988.
- Bilitza, D., S. Radicella, B. Reinisch, J. Adeniyi, M. Mosert, S. Zhang, and O. Obrou (2000), New B0 and B1 models for IRI. *Adv. Space Res.* 25(1): 89-95.
- Bilitza, D., V. Truhlik, P. Richards, T. Abe, and L. Triskova, Solar cycle variation of mid-latitude electron density and temperature: Satellite measurements and model calculations, *Adv. Space Res.*, 39, #5, 779-789, doi: 10.1016/j.asr.2006.11.022, 2007.
- Bilitza, D, and Reinisch, B.W. (2008), International Reference Ionosphere 2007: Improvements and new parameters. *Adv. Space Res.* 42(4): 599-609. doi:10.1016/j.asr.2007.07.048.
- CCIR, Atlas of Ionospheric Characteristics, Comité Consultatif International des Radiocommunications, Report 340-1, 340-6, Genève, Switzerland, (ISBN 92-61-04417-4), 1966.
- Fernandez J.R., C. J. Mertens, D. Bilitza, X. Xu, J.M. Russell III, and M.G. Mlynczak (2010), Feasibility of developing an ionospheric E-region electron density storm model using TIMED/SABER measurements. *Adv. Space Res.* 46(8): 1070-1077. doi:10.1016/j.asr.2010.06.008.
- Fox M.W. and L.F. McNamara, Improved World-wide Maps of Monthly Median foF2, *Journal of Atmospheric and Solar-Terrestrial Physics*, 50, 12, pp. 1077-1086, 1988.
- Fuller-Rowell, T.J., E. Araujo-Pradere, and M.V. Codrescu (2000), An empirical ionospheric storm-time correction model. *Adv. Space Res.* 25(1): 139-146.
- Galkin, I.A., G.M. Khmyrov, A.V. Kozlov, B.W. Reinisch, X. Huang, and V.V. Paznukhov, The ARTIST 5, in *Radio Sounding and Plasma Physics*, AIP Conf. Proc. 974, 150-159, 2008.
- Galkin, I.A., B.W. Reinisch, and X. Huang, Assimilative IRI with Real-Time GIRO Input, Proc. 13th Intern. Ionosph. Effects Symp. IES-2011, Alexandria, VA, May 17-19, 2011, pp. 1-8.
- Galkin, I.A., B.W. Reinisch, X. Huang, and D. Bilitza, Assimilation of GIRO data in Real-Time IRI: Progress Report, International Reference Ionosphere Workshop IRI-2011, Hermanus, South Africa, October 10-14, 2011.
- Gulyaeva, T. (1987) Progress in ionospheric informatics based on electron density profile analysis of ionograms. *Adv. Space Res.* 7(6): 39-48.

- IGRF (2010) International Geomagnetic Reference Field, Version 11, <http://www.ngdc.noaa.gov/IAGA/vmod/igrf.html>.
- Jones W.B. and R. M. Gallet, "Representation of Diurnal and Geographical Variations of Ionospheric Data by Numerical Methods," *Telecommunication Journal*, 29, pp. 129-149, 1962.
- Jones, W.B., R.P. Graham, and M. Leftin, "Advances in Ionospheric Mapping by Numerical Methods", *ESSA Technical Report ERL 107-ITS 75*, US Government Printing Office, Washington DC, USA, 1969.
- Liu R.Y., P.A. Smith, and J.W. King, "A New Solar Index Which Leads to Improved foF2 Predictions Using the CCIR Atlas, *Telecommunication Journal*, 50, 8, pp. 408-414, 1983.
- McKinnell L.A. and A.W.V. Poole, Neural network based ionospheric modelling over the South African region, *South African Journal of Science*, 100, pp. 519-523, 2004.
- McKinnell L.A. and E.O. Oyeyemi, "Progress towards a new global foF2 model for the International Reference Ionosphere (IRI)", *Advances in Space Research*, doi: 10.1016/j.asr.2008.09.035, 2009.
- McKinnell, L.A. and E.O. Oyeyemi, Equatorial predictions from a new neural network based global foF2 model, *Advances in Space Research*, doi: 10.1016/j.asr.2010.06.003, 46, pp. 1016-1023, 2010.
- Mertens, C., J. Winick, J. Russell III, M. Mlynczak, D. Evans, D. Bilitza, and X. Xu (2007), Empirical storm-time correction to the International Reference Ionosphere model E-region electron and ion density parameterizations using observations from TIMED/SABER. Proc. SPIE Remote Sensing of Clouds and Atmosphere XII: 67451L. doi: 10.1117/12.737318.
- Oyeyemi E.O., L.A. McKinnell, and A.W.V. Poole, "Neural network based prediction techniques for global modelling of M(3000)F2 ionospheric parameter", *Advances in Space Research*, doi:10.1016/j.asr.2006.09.038, 39, 5, pp. 643-650, 2007.
- Oyeyemi E.O. and L.A. McKinnell, "A new global F2 peak electron density model for the International Reference Ionosphere (IRI)", *Advances in Space Research*, doi: 10.1016/j.asr.2007.10.031, 42, 4, pp. 645-658, 2008.
- Picone, J.M., A.E. Hedin, D.P. Drob, and A.C. Aikin, NRLMSISE-00 empirical model of the atmosphere: Statistical comparisons and scientific issues, *J. Geophys. Res.*, 107(A12), 1468, doi:10.1029/2002JA009430, 2002.
- Rawer, K., D. Bilitza, and S. Ramakrishnan, Goals and status of the International Reference Ionosphere, *Rev. Geophys.* 16, pp. 177-181, 1978a.
- Rawer, K., D. Bilitza, and S. Ramakrishnan, *International Reference Ionosphere*, International Union of Radio Science (URSI), Brussels, Belgium, 1978b.
- Reinisch, B.W. and I.A. Galkin, Global Ionospheric Radio Observatory (GIRO), *Earth, Planets and Space*, vol. 63 No. 4, pp. 377-381, 2011.
- Richards, P. G., D. Bilitza, and D. Voglozin (2010), Ion density calculator (IDC): A new efficient model of ionospheric ion densities, *Radio Sci.*, 45, RS5007, doi:10.1029/2009RS004332.
- Rush, C., M. Fox, D. Bilitza, K. Davies, L. McNamara, F. Stewart, and M. PoKempner, "Ionospheric Mapping – An Update of foF2 Coefficients," *Telecommunication Journal*, 56, pp. 179-182, 1989.
- Scherliess, L., R.W. Schunk, J.J. Sojka, D.C. Thompson, and L. Zhu, The USU GAIM Gauss-Markov Kalman Filter Model of the Ionosphere: Model Description and Validation *J. Geophys. Res.*, 111, A11315, doi:10.1029/2006JA011712, 2006.
- Szuszczewicz, E. *et al.* (1993), Measurements and empirical model comparisons of F-region characteristics and auroral boundaries during the solstitial SUNDAIL campaign of 1987. *Ann. Geophysicae* 11: 601-613.
- Truhlik V., L. Triskova, D. Bilitza, and Katerina Podolska, Variations of daytime and nighttime electron temperature and heat flux in the upper ionosphere, topside ionosphere and lower plasmasphere for

low and high solar activity, J. Atmos. Sol.-Terr. Phys. 71, 2055–2063, doi:10.1016/j.jastp.2009.09.013, 2009.

Truhlik, V., D. Bilitza, and L. Triskova, A new global empirical model of the electron temperature with inclusion of the solar activity variations for IRI, submitted to EPS, 2011.

Zhang, Y., and L.J. Paxton (2008), An empirical Kp-dependent global auroral model based on TIMED/GUVI data. J. Atmos. Solar-Terr. Phys. 70: 1231-1242. doi:10.1016/j.jastp.2008.03.008.

Zhang, Y., L.J. Paxton, and D. Bilitza (2010), Near real-time assimilation of auroral peak E-region density and equatorward boundary in IRI. Adv. Space Res. 46(8): 1055-1063. doi:10.1016/j.asr.2010.06.029.

3 NeQuick2 electron density model

3.1 Background

NeQuick 2 is the latest version of the NeQuick ionosphere electron density model developed at the Aeronomy and Radiopropagation Laboratory of the Abdus Salam International Centre for Theoretical Physics (ICTP) – Trieste, Italy with the collaboration of the Institute for Geophysics, Astrophysics and Meteorology of the University of Graz, Austria. The NeQuick is a quick-run ionospheric electron density model particularly designed for transionospheric propagation applications.

To describe the electron density of the ionosphere up to the peak of the F2 layer, the NeQuick uses a profile formulation which includes five semi-Epstein layers with modelled thickness parameters. Three profile anchor points are used: the E layer peak, the F1 peak and the F2 peak, that are modelled in terms of the ionosonde parameters foE , $foF1$, $foF2$ and $M(3000)F2$. These values can be modelled (e.g. ITU-R coefficients for $foF2$, $M3000$) or experimentally derived. A semi-Epstein layer represents the model topside with a height – dependent thickness parameter empirically determined. The NeQuick package includes routines to evaluate the electron density along any ray-path and the corresponding TEC by numerical integration.

3.2 The NeQuick electron density model

This section describes how to compute the NeQuick electron density for a given location (identified by the coordinates h , φ , λ) at a given time (month, UT) using Rz or F10.7 parameters (provided or not by the user).

Inputs:

height h (km), latitude φ (degrees), longitude λ (degrees), month $month$, Universal Time UT (hours and decimals), Rz or F10.7.

Output:

electron density N (m^{-3}).

3.2.1 The Epstein function

Since to compute the NeQuick electron density profile, the Epstein function is used, we recall its formulation:

$$Epst(X, Y, Z, W) = \frac{X * \exp\left(\frac{W - Y}{Z}\right)}{\left(1 + \exp\left(\frac{W - Y}{Z}\right)\right)^2} \quad (1)$$

3.2.2 Constants used

For the calculation of the slant TEC, some constant parameters are used and they are summarized in Table 1.

TABLE 1
Constants definition

Symbol	Constant description	Value	Units
DR	Degree to radiant conversion factor	$\pi/180$	rad/degrees
RD	Radiant to degree conversion factor	$180/\pi$	rad/degrees
χ_0	Zenith angle at night-day transition	86.23	degrees
R_E	Earth mean radius	6371.2	km

3.2.3 Auxiliary parameters

To compute the NeQuick electron density, several auxiliary parameters are preliminarily evaluated through specific modules. In this section the parameter formulation is given.

3.2.3.1 Local Time

Compute local time LT (in hours and decimals) for the location considered.

Inputs:

longitude λ (degrees), Universal Time UT (hours and decimals).

Output:

local time LT (hours and decimals).

$$LT = UT + \lambda/15 \quad (2)$$

3.2.3.2 Modip map

NeQuick 2.1 uses a map of modified dip or Modip to get the magnetic coordinates needed by the model for computing the F2 layer peak and F1 layer height.

Modip, which was first introduced by Rawer [1963, RD4] is defined by:

$$\tan \mu = \frac{I}{\sqrt{\cos \varphi}} \quad (3)$$

in which I is magnetic inclination (degrees) at 300 km and φ is the latitude (degrees) of the considered location. NeQuick 2.1 model uses a grid of modip values contained in the file *modip.asc*.

The file *modip.asc* contains the values of modip on a geocentric grid from 90°S to 90°N with steps of 1 degree in latitude and from 180°W to 180°E with steps of 2 degrees in longitude. In particular the first 181 numbers are the modip values for latitude (degrees) = -90.0 (and longitude (degrees) = -180, -178 ..., 180), etc.; the last 181 numbers are the modip values for latitude (degrees) = +90.0 (and longitude (degrees) = -180, -178 ..., 180).

To compute the modip value in a point at latitude φ and longitude λ , a third order interpolation is applied using surroundings grid values.

The NeQuick interpolation function is described in § 3.3.3.1.

For computational purposes, it is therefore convenient to describe how the modip values are stored in a grid D and how additional rows and columns are defined in order to apply the interpolation algorithm near the poles or near longitude (degrees) = 180.

3.2.3.2.1 Store the modip.asc values in an array

$$D: \quad d_{i,j} \quad i = 1, \dots, 181; \quad j = 0, \dots, 180; \quad (4)$$

being i the index of latitude and j the index of longitude.

Define additional rows:

$$d_{0,j} = d_{2, \text{mod}(j+90, 180)} \quad (5)$$

$$d_{182,j} = d_{180, \text{mod}(j+90, 180)} \quad (6)$$

$$d_{183,j} = d_{179, \text{mod}(j+90, 180)} \quad (7)$$

with $j = 0, \dots, 180$ and being $\text{mod}(a,b)$ the remainder on division of a by b .

Define additional columns:

$$d_{i,-1} = d_{i,179} \quad (8)$$

$$d_{i,181} = d_{i,1} \quad (9)$$

with $i = 0, \dots, 183$.

Therefore now the matrix D becomes:

$$D: \quad d_{i,j} \quad i = 0, \dots, 183; \quad j = -1, \dots, 181; \quad (10)$$

3.2.3.2.2 Compute the Modip

Inputs:

latitude φ (degrees), longitude λ (degrees), array D (of dip latitude values).

Output:

Modip μ (degrees)

The selection of the interpolation grid-points is done by computing:

$$l = \text{int}\left(\frac{\lambda + 180}{2}\right) - 2 \quad (11)$$

If $l < 0$ use

$$l = l + 180 \quad (12)$$

If $l > 177$ use

$$l = l - 180 \quad (13)$$

Compute

$$a = \frac{\varphi + 90}{1} + 1 \quad (14)$$

$$x = a - \text{int}(a) \quad (15)$$

$$i = \text{int}(a) - 2 \quad (16)$$

For $k = 1, 4$; for $j = 1, 4$ build the $z_{j,k}$ as:

$$z_{j,k} = d_{i+j,l+k} \quad (17)$$

For $k = 1,4$ compute

$$z_k = z_x(z_{1,k}, z_{2,k}, z_{3,k}, z_{4,k}, x) \quad (18)$$

using the interpolation function described in § 3.3.3.1.

Finally compute

$$b = \frac{\lambda + 180}{2} \quad (19)$$

$$y = b - \text{int}(b) \quad (20)$$

and using the interpolation function described in § 3.3.3.1, calculate

$$\mu = z_x(z_1, z_2, z_3, z_4, y) \quad (21)$$

3.2.3.3 Solar declination

Compute $\sin\delta_{Sun}$, $\cos\delta_{Sun}$, the sine and cosine of the solar declination.

Inputs:

month mth , Universal Time UT (h)

Outputs:

$\sin\delta_{Sun}$, $\cos\delta_{Sun}$,

Compute day of year at the middle of the month:

$$d_y = 30.5 * mth - 15 \quad (22)$$

Compute time (days):

$$t = d_y + (18 - UT) / 24 \quad (23)$$

Compute the argument:

$$a_m = (0.9856t - 3.289) * DR \quad (24)$$

$$a_l = a_m + [1.916\sin(a_m) + 0.020\sin(2a_m) + 282.634] * DR \quad (25)$$

Finally compute sine and cosine of solar declination:

$$\sin \delta_{Sun} = 0.39782 \sin a_l \quad (26)$$

$$\cos \delta_{Sun} = \sqrt{1 - \sin^2 \delta_{Sun}} \quad (27)$$

3.2.3.4 Solar zenith angle

Compute solar zenith angle χ (degrees) for the given location.

Inputs:

latitude φ (degrees), local time LT (h), $\sin\delta_{Sun}$, $\cos\delta_{Sun}$,

Output:

solar zenith angle χ (degrees).

Compute

$$\cos_{\chi} = \sin(\varphi * DR) * \sin\delta_{Sun} + \cos(\varphi * DR) * \cos\delta_{Sun} \cos\left(\frac{\pi}{12}(12 - LT)\right) \quad (28)$$

$$\chi = RD * \text{atan2}\left(\sqrt{1 - \cos\chi^2}, \cos\chi\right) \quad (29)$$

3.2.3.5 Effective solar zenith angle

Compute the effective solar zenith angle χ_{eff} (degrees) as a function of the solar zenith angle χ (degrees) and the solar zenith angle at day night transition χ_0 (degrees).

Inputs:

Solar zenith angle χ (degrees), χ_0 (degrees)

Output:

Effective solar zenith angle χ_{eff} (degrees).

Being

$$\chi_0 = 86.23^\circ \quad (30)$$

Then

$$\chi_0 = \frac{\chi + [90 - 0.24 \exp(20 - 0.2 * \chi)] \exp[12(\chi - \chi_0)]}{1 + \exp[12(\chi - \chi_0)]} \quad (31)$$

3.2.4 Model parameters

In the following point, model peak parameter and auxiliary parameter values will be calculated.

3.2.4.1 foE and NmE

To compute the E layer critical frequency foE (MHz) at a given location, in addition to the effective solar zenith angle χ_{eff} , a season dependent parameter has to be computed.

Inputs:

latitude φ (degrees), flux flx , effective solar zenith angle χ_{eff} (degrees), month nth .

Output:

foE (MHz).

Define the $seas$ parameter as a function of the month of the year as follows:

$$\text{If } nth = 1, 2, 11, 12 \text{ then } seas = -1 \quad (32)$$

$$\text{If } nth = 3, 4, 9, 10 \text{ then } seas = 0 \quad (33)$$

$$\text{If } nth = 5, 6, 7, 8 \text{ then } seas = 1 \quad (34)$$

Introduce the latitudinal dependence:

$$ee = \exp(0.3 * \varphi) \quad (35)$$

$$seasp = seas * \frac{ee - 1}{ee + 1} \quad (36)$$

$$foE = \sqrt{(1.112 - 0.019 * seasp)^2 * \sqrt{flx} * [\cos(\chi_{\text{eff}} * DR)]^{0.6} + 0.49} \quad (37)$$

The E layer maximum density NmE (10^{11} m^{-3}) as a function of foE (MHz) is computed as:

$$NmE = 0.124 * foE^2 \quad (38)$$

3.2.4.2 $foF1$ and $NmF1$

The F1 layer critical frequency $foF1$ (MHz) in NeQuick 2.1 has been reformulated [Leitinger *et al.*, 2005, RD3].

Inputs:

E layer critical frequency foE (MHz), F2 layer critical frequency $foF2$ (MHz),

Output:

$$foF1 \text{ (MHz)} = \begin{cases} 0 & \text{if } foE < 2 \\ 1.4foE & \text{if } foE \geq 2 \text{ and } 1.4foE \leq 0.85foF2 \\ 0.85 \cdot 1.4foE & \text{if } 1.4foE > 0.85foF2 \end{cases} \quad (39)$$

The F layer maximum density $NmF1$ (10^{11} m^{-3}) as a function of $foF1$ (MHz) is computed as:

$$NmF1 = 0.124 * foF1^2 \quad (40)$$

3.2.4.3 $foF2$ and $NmF2$; $M(3000)F2$

To compute $foF2$ and $M(3000)F2$, the NeQuick model uses the ITU-R (formerly CCIR) coefficients [ITU-R, 1997]. These coefficients are stored in the ccirXX.asc files and are the spherical harmonic coefficients representing the development of monthly median $foF2$ and $M(3000)F2$ all over the world. The coefficients correspond to low ($R_{12} = 0$) and high ($R_{12} = 100$) solar activity conditions. Therefore they have to be interpolated (or extrapolated) to obtain the set of coefficients corresponding to the required solar activity.

Each file ccirXX.asc contains 2858 values sequentially organized as follows: $\{f2_{1,1,1}, f2_{1,1,2}, \dots, f2_{1,1,13}, f2_{1,2,1}, f2_{1,2,2}, \dots, f2_{1,2,13}, \dots, f2_{1,76,1}, f2_{1,76,2}, \dots, f2_{1,76,13}, f2_{2,1,1}, \dots, f2_{2,1,2}, \dots, f2_{2,1,13}, f2_{2,2,1}, f2_{2,2,2}, \dots, f2_{2,2,13}, \dots, f2_{2,76,1}, f2_{2,76,2}, \dots, f2_{2,76,13}, fm3_{1,1,1}, fm3_{1,1,2}, \dots, fm3_{1,1,9}, fm3_{1,2,1}, fm3_{1,2,2}, \dots, fm3_{1,2,9}, \dots, fm3_{1,49,1}, fm3_{1,49,2}, \dots, fm3_{1,49,9}, fm3_{2,1,1}, fm3_{2,1,2}, \dots, fm3_{2,1,9}, fm3_{2,2,1}, fm3_{2,2,2}, \dots, fm3_{2,2,9}, \dots, fm3_{2,49,1}, fm3_{2,49,2}, \dots, fm3_{2,49,9}\}$. (The notation used will become self evident after the definition of the F2 and Fm3 arrays).

The coefficients of a ccirXX.asc file have to be stored in two 3-D arrays, $F2$ and $Fm3$, as indicated in the next section.

3.2.4.3.1 Store ccirXX.asc values

Input:

Month mth

Outputs:

$F2$, $Fm3$

Select the file name to read:

$$XX = m + 10 \quad (41)$$

(e.g. ccir21.asc for November) and store the file content in the two arrays of coefficients:

coefficients for $foF2$

$$F2: \quad f2_{i,j,k} \quad i = 1,2; \quad j = 1,\dots,76; \quad k = 1,\dots,13 \quad (42)$$

coefficients for $M(3000)F2$

$$Fm3: \quad fm3_{i,j,k} \quad i = 1,2; \quad j = 1,\dots,49; \quad k = 1,\dots,9 \quad (43)$$

3.2.4.3.2 Interpolate ITU-R coefficients for R_{12}

Compute $AF2$, the array of interpolated coefficients for $foF2$ and $Am3$, the array of interpolated coefficients for $M(3000)F2$.

Inputs:

$F2, Fm3, R_{12}$

Outputs:

$AF2, Am3$

Compute the array of interpolated coefficients for $foF2$:

$$AF2: \quad af2_{j,k} \quad j = 1,\dots,76; \quad k = 1,\dots,13 \quad (44)$$

$AF2$ elements are calculated by linear combination of the elements of $F2$:

$$af2_{j,k} = f2_{1,j,k} \left(1 - \frac{R_{12}}{100}\right) + f2_{2,j,k} \frac{R_{12}}{100} \quad j = 1,\dots,76; \quad k = 1,\dots,13 \quad (45)$$

Compute the array of interpolated coefficients for $M(3000)F2$:

$$Am3: \quad am3_{j,k} \quad j = 1,\dots,49; \quad k = 1,\dots,9 \quad (46)$$

$Am3$ elements are calculated by linear combination of the elements of $Fm3$:

$$am3_{j,k} = fm3_{1,j,k} \left(1 - \frac{R_{12}}{100}\right) + fm3_{2,j,k} \frac{R_{12}}{100} \quad j = 1,\dots,49; \quad k = 1,\dots,9 \quad (47)$$

3.2.4.3.3 Compute Fourier time series for $foF2$ and $M(3000)F2$

Inputs:

Universal Time UT (h), arrays of interpolated ITU-R coefficients $AF2, Am3$

Outputs:

$CF2, Cm3$, vectors of coefficients for Legendre calculation for $foF2$ and $M(3000)F2$.

Vector $CF2$ has 76 elements:

$$CF2: \quad cf2_l \quad l = 1,\dots,76 \quad (48)$$

Vector $Cm3$ has 49 elements:

$$Cm3: \quad cm3_l \quad l = 1,\dots,49 \quad (49)$$

Compute the time argument:

$$T = (15UT - 180)DR \quad (50)$$

For $i = 1,\dots,76$ calculate the Fourier time series for $foF2$:

$$cf2_i = af2_{i,1} + \sum_{k=1}^6 [af2_{i,2k} \sin(kT) + af2_{i,2k+1} \cos(kT)] \quad (51)$$

For $i = 1,\dots,49$ calculate the Fourier time series for $M(3000)F2$:

$$cm3_i = am3_{i,1} + \sum_{k=1}^4 [am3_{i,2k} \sin(kT) + am3_{i,2k+1} \cos(kT)] \quad (52)$$

3.2.4.3.4 Compute $foF2$ and $M(3000)F2$ by Legendre calculation

Inputs:

Modip μ (degrees), latitude φ (degrees), longitude λ (degrees), vector $CF2$ of the coefficients for Legendre combination for $foF2$, vector $Cm3$ of the coefficients for Legendre combination for $M(3000)F2$.

Outputs:

$foF2$ (MHz), $M(3000)F2$

Define vectors containing sine and cosines of coordinates:

$$M: \quad m_k \quad k = 1, \dots, 12 \quad (53)$$

$$P: \quad p_n \quad n = 2, \dots, 9 \quad (54)$$

$$S: \quad s_n \quad n = 2, \dots, 9 \quad (55)$$

$$C: \quad c_n \quad n = 2, \dots, 9 \quad (56)$$

Compute modip coefficients:

$$m_1 = 1 \quad (57)$$

and for $k = 2, \dots, 12$

$$m_k = \sin^{k-1}(\mu * DR) \quad (58)$$

Compute latitude and longitude coefficients:

and for $n = 2, \dots, 9$

$$p_n = \cos^{n-1}(\varphi * DR) \quad (59)$$

$$s_n = \sin((n-1)\lambda * DR) \quad (60)$$

$$c_n = \cos((n-1)\lambda * DR) \quad (61)$$

Compute $foF2$

Order 0 term:

$$foF2_1 = \sum_{k=1}^{12} cf2_k m_k \quad (62)$$

having the increased Legendre grades for $foF2$ in a vector:

$$Q: \quad q_n \quad n = 1, \dots, 9 \quad (63)$$

$$Q = (12, 12, 9, 5, 2, 1, 1, 1) \quad (64)$$

for computational need define also:

$$K: \quad k_n \quad n = 1, \dots, 9 \quad (65)$$

$$k_1 = 12 \quad (66)$$

and for $n = 2, \dots, 9$

$$k_n = k_{n-1} + q_n \quad (67)$$

for $n = 2, \dots, 9$ compute the higher order terms:

$$foF2_n = \sum_{k=1}^{q_n} \left(cf2_{k_n+2k-1} c_n + cf2_{k_n+2k} s_n \right) m_k p_n \quad (68)$$

Finally sum the terms to obtain $foF2$:

$$foF2 = \sum_{n=1}^9 foF2_n \quad (69)$$

Compute $M(3000)F2$

Order 0 term:

$$M(3000)F2_0 = \sum_{k=1}^5 cm3_k m_k \quad (70)$$

having the increased Legendre grades for $M(3000)F2$ in a vector:

$$R: \quad r_n \quad n = 1, \dots, 7 \quad (71)$$

$$R = (7, 8, 6, 3, 2, 1, 1) \quad (72)$$

for computational need define also:

$$H: \quad h_n \quad n = 1, \dots, 7 \quad (73)$$

$$k_1 = 12 \quad (74)$$

and for $n = 2, \dots, 7$

$$k_n = k_{n-1} + q_n \quad (75)$$

for $n = 2, \dots, 7$, compute the higher order terms:

$$M(3000)F2_n = \sum_{k=1}^{r_n} \left(cm3_{h_n+2k-1} c_n + cm3_{h_n+2k} s_n \right) m_k p_n \quad (76)$$

Finally sum the terms:

$$M(3000) = \sum_{n=1}^7 M(3000)F2_n \quad (77)$$

To compute $NmF2$ use:

$$NmF2 = 0.124 * foF2^2 \quad (78)$$

where $NmF2$ is in (10^{11}m^{-3}).

3.2.4.4 hmE

The E layer maximum density height hmE (km) is defined as a constant:

$$hmE = 120 \quad (79)$$

3.2.4.5 $hmF2$

Compute the F2 layer maximum density height $hmF2$ (km).

Inputs:

foE (MHz), $foF2$ (MHz), $M(3000)F2$.

Output:

$hmF2$ (km).

$$hmF2 = \frac{1490M \sqrt{\frac{0.0196\sqrt{M^2+1}}{1.2967\sqrt{M^2-1}}}}{M + \Delta M} - 176 \quad (80)$$

where:

$$M = M(3000)F2 \quad (81)$$

$$\Delta M = -0.012 \quad \text{if} \quad foE < 10^{-30} \quad (82)$$

$$\Delta M = \frac{0.253}{\rho - 1.215} - 0.012 \quad \text{if} \quad foE \geq 10^{-30} \quad (83)$$

and the ratio ρ is computed as:

$$\rho = \frac{\frac{foF2}{foE} \exp[20(\frac{foF2}{foE} - 1.75)] + 1.75}{\exp[20(\frac{foF2}{foE} - 1.75)] + 1} \quad (84)$$

3.2.4.6 *hmF1*

Compute the *F1* layer maximum density height *hmF1* (km):

Inputs:

hmE (km), *hmF2* (km).

Output:

hmF1 (km).

$$hmF1 = \frac{hmE + hmF2}{2} \quad (85)$$

3.2.4.7 *B2_{bot}*

Compute the thickness parameter *B2_{bot}* (km).

Inputs:

NmF2 (10^{11} m^{-3}), *foF2* (MHz), *M(3000)F2*.

Output:

B2_{bot} (km).

$$B2_{bot} = \frac{0.385NmF2}{0.01 \exp[-3.467 + 1.714 \ln(foF2) + 2.02 \ln(M)]} \quad (86)$$

where

M = *M(3000)F2* as already indicated in equation (82).

3.2.4.8 *A1*

Compute the *F2* layer amplitude *A1* (10^{11} m^{-3}).

Inputs:

NmF2 (10^{11} m^{-3}).

Output:

A1 (10^{11} m^{-3}).

$$A1 = 4 * NmF2 \quad (87)$$

3.2.4.9 A2

Compute the F1 layer amplitude A2 (10^{11} m^{-3}).

Inputs:

$NmF1$ (10^{11} m^{-3}), $A1$ (10^{11} m^{-3}), $hmF2$ (km), $B2_{bot}$ (km), $hmF1$ (km).

Output:

A2 (10^{11} m^{-3}).

First compute the auxiliary parameter

$$A2a = 4.0(NmF1 - Epst(A1, hmF2, B2_{bot}, hmF1)) \quad (88)$$

where the function $Epst$ is the one defined in § 3.2.1.

Then compute

$$A2 = \frac{A2a * \exp[60 * (A2a - 0.005)] + 0.05}{1 + \exp[60 * (A2a - 0.005)]} \quad (89)$$

3.2.4.10 B1_{top}

Compute the thickness parameter $B1_{top}$ (km).

Inputs:

hmE (km), $hmF2$ (km)

Output:

$B1_{top}$ (km).

The thickness parameter $B1_{top}$ (km) is given by:

$$B1_{top} = 0.3(hmF2 - hmF1) \quad (90)$$

3.2.4.11 B1_{bot}

Compute the thickness parameter $B1_{bot}$ (km).

Inputs:

$hmF1$ (km), hmE (km)

Output:

$B1_{bot}$ (km).

$$B1_{bot} = 0.5(hmF1 - hmE) \quad (91)$$

3.2.4.12 A3

Compute the E layer amplitude A3 (10^{11} m^{-3}).

Inputs:

NmE (10^{11} m^{-3}), A2 (10^{11} m^{-3}), $hmF1$ (km), $hmF2$ (km), hmE (km), $B1_{bot}$ (km), $B2_{bot}$ (km).

Output:

A3 (10^{11} m^{-3}).

First compute the auxiliary parameter A3a:

$$A3a = 4.0 * (NmE - Epst(A2, hmF1, B1_{bot}, hmE) - Epst(A1, hmF2, B2_{bot}, hmE)) \quad (92)$$

where the function $Epst$ is the one defined in § 3.2.1.

Then compute:

$$A3 = \frac{A3a * \exp[60 * (A3a - 0.005)] + 0.005}{1 + \exp[60 * (A3a - 0.005)]} \quad (93)$$

3.2.4.13 BE_{top}

Compute the thickness parameter BE_{top} (km).

Inputs:

$hmF1$ (km), hmE

Output:

BE_{top} (km).

$$BE_{top} = \max(0.5(hmF1 - hmE), 7) \quad (94)$$

3.2.4.14 BE_{bot}

Compute the thickness parameter BE_{bot} (km).

$$BE_{bot} = 5 \quad (95)$$

3.2.4.15 Shape parameter k

Compute the shape parameter k .

Inputs:

$foF2$ (MHz), $hmF2$ (km), $B2_{bot}$ (km).

Output:

k .

Compute

$$k = 3.22 - 0.0538 foF2 - 0.00664 hmF2 + 0.113 \frac{hmF2}{B2_{bot}} + 0.00257 R_{12} \quad (96)$$

a lower limiting value of 1 is imposed on k .

3.2.4.16 H_0

Compute the topside thickness parameter H_0 (km).

Inputs:

$B2_{bot}$ (km), k

Output:

H_0 (km)

Compute

$$H_0 = k B2_{bot} \quad (97)$$

3.3 Electron density computation

To compute the electron density $N = N(h, \varphi, \lambda, l, flx, mth, UT)$ at a given point (identified by the coordinates h, φ, λ) and time ($month, UT$) using a given F10.7, all NeQuick parameters have to be

evaluated. Nevertheless two different modules have to be used accordingly to the height considered. In particular

if

$$h \leq hmF2 \quad (98)$$

the bottomside electron density has to be computed using the algorithm illustrated in § 3.3.1.

if

$$h > hmF2 \quad (99)$$

the topside electron density has to be computed using the algorithm illustrated in § 3.3.2.

3.3.1 The bottomside electron density

Compute the electron density N of the bottomside ($h \leq hmF2$).

Inputs:

height h (km), A_1 (10^{11} m^{-3}), A_2 (10^{11} m^{-3}), A_3 (10^{11} m^{-3}), $hmF2$ (km), $hmF1$ (km), hmE (km), $B2_{bot}$ (km), $B1_{top}$ (km), $B1_{bot}$ (km), BE_{top} (km), BE_{bot} (km).

Output:

(bottomside) electron density N (m^{-3}).

Select the relevant B parameters for the current height:

$$BE = \begin{cases} BE_{top} & \text{if } h > hmE \\ BE_{bot} & \text{if } h \leq hmE \end{cases} \quad (100)$$

$$BF1 = \begin{cases} BF1_{top} & \text{if } h > hmF1 \\ BF1_{bot} & \text{if } h \leq hmF1 \end{cases} \quad (101)$$

Compute the exponential arguments for each layer:

$$\alpha_1 = \frac{h - hmF2}{B2_{bot}} \quad (102)$$

$$\alpha_2 = \frac{h - hmF1}{BF1} \exp\left(\frac{10}{1 + |h - hmF2|}\right) \quad (103)$$

$$\alpha_3 = \frac{h - hmE}{BE} \exp\left(\frac{10}{1 + |h - hmF2|}\right) \quad (104)$$

If $h < 90$ km, for each $i = 1, 3$ compute:

$$\alpha_i = \alpha_i * (5 + 90 - h) / 5 \quad (105)$$

$$s_i = \begin{cases} 0 & \text{if } |\alpha_i| > 25 \\ A_i \frac{\exp(\alpha_i)}{(1 + \exp(\alpha_i))^2} & \text{if } |\alpha_i| \leq 25 \end{cases} \quad (106)$$

Then compute the electron density as:

$$N = (s_1 + s_2 + s_3) \times 10^{11} \quad (107)$$

3.3.2 The topside electron density

Compute the electron density N of the topside ($h > hmF2$).

Inputs:

height h (km), $NmF2$ (10^{11} m^{-3}), $hmF2$ (km), H_0 (km).

Output:

(topside) electron density N (m^{-3}).

Define the constant parameters g and r as:

$$g = 0.125 \quad (108)$$

$$r = 100 \quad (109)$$

compute the z argument as:

$$z = \frac{h - hmF2}{H_0 \left[1 + \frac{rg(h - hmF2)}{rH_0 + g(h - hmF2)} \right]} \quad (110)$$

Eventually

$$N(h) = \frac{4NmF2}{(1 + \exp(z))^2} \exp(z) \quad (111)$$

3.3.3 Auxiliary routines

3.3.3.1 Third order interpolation function $z_x(z_1, z_2, z_3, z_4, x)$

Be $P1 = (-1, z_1)$, $P2 = (0, z_2)$, $P3 = (1, z_3)$, $P4 = (2, z_4)$:

If $P = (x, z_x)$, to compute the interpolated value z_x at the position x , being $x \in [0, 1)$, the following algorithm is applied.

Inputs: z_1, z_2, z_3, z_4, x

Outputs: z_x .

If $|x^2| \leq 10^{10}$

$$z_x = z_2 \quad (112)$$

Otherwise compute:

$$\delta = x^2 - 1 \quad (113)$$

$$g_1 = z_3 + z_2 \quad (114)$$

$$g_2 = z_3 - z_2 \quad (115)$$

$$g_3 = z_4 + z_1 \quad (116)$$

$$g_4 = \frac{z_4 - z_1}{3} \quad (117)$$

$$a_0 = 9g_1 - g_3 \quad (118)$$

$$a_1 = 9g_2 - g_4 \quad (119)$$

$$a_2 = g_3 - g_1 \quad (120)$$

$$a_3 = g_4 - g_2 \quad (121)$$

$$z_x = \frac{1}{16} (a_0 + a_1\delta + a_2\delta^2 + a_3\delta^3) \quad (122)$$

3.4 TEC calculation

To compute the slant TEC along a straight line between a point P_1 and a point P_2 , the NeQuick electron density N has to be evaluated on a point P defined by the coordinates $\{h, \varphi, \lambda\}$ along the ray-path.

It is a choice depending on receiver computation capabilities to identify the number of points where N is to be evaluated, in order to obtain a sufficient accuracy for a subsequent integration, leading to slant TEC.

The Earth is assumed to be a sphere with a radius of 6371.2 km.

For computational efficiency, if the latitude of P_1 and P_2 are close to each other and the longitude of P_1 and P_2 are close to each other (as indicated in equation (127)):

$$\begin{cases} |\varphi_2 - \varphi_1| < 10^{-5} \\ |\lambda_2 - \lambda_1| < 10^{-5} \end{cases} \quad (123)$$

the vertical integration algorithm has to be used, as described in § 3.4.1; otherwise use the slant integration algorithm as described in § 3.4.2.

During the TEC computation, the electron density at the point P has to be evaluated as indicated in § 2.2, while the calculation of the coordinates of the point P along the ray-path will be described in § 3.4.1.1 if a vertical ray-path is considered and in § 3.4.2.3 if a slant ray-path is considered.

3.4.1 Vertical TEC calculation

To compute NeQuick vertical TEC, first compute all profile parameters hmE , $hmF1$, $hmF2$, $A1$, $A2$, $A3$, $B2_{bot}$, $B1_{top}$, $B1_{bot}$, BE_{top} , BE_{bot} , $NmF2$, H_0 , then compute the integration of the electron density (bottomside or topside) as a function of height:

$$TEC = \int N(h)dh \quad (124)$$

being:

$$h_1 = r_1 - R_E \quad (125)$$

$$h_2 = r_2 - R_E \quad (126)$$

3.4.1.1 Vertical TEC numerical integration

Inputs:

- Integration endpoints h_1 (km), h_2 (km)
- Integration accuracy ε
- Model parameters A_1 (10^{11} m^{-3}), A_2 (10^{11} m^{-3}), A_3 (10^{11} m^{-3}), $hmF2$ (km), $hmF1$ (km), hmE (km), $B2_{bot}$ (km), $B1_{top}$ (km), $B1_{bot}$ (km), BE_{top} (km), BE_{bot} (km), $NmF2$ (m^{-3}), H_0 (km)

Output:

- TEC (10^{15} m^{-2})

Being φ , λ , and all model parameters fixed during the integration, in the following a simplified notation is used:

$$N(h) = \begin{cases} \text{bottomside } N & \text{if } h \leq hmF2 \\ \text{topside } N & \text{if } h > hmF2 \end{cases} \quad (127)$$

$N(h)$ is computed using the algorithms described in § 3.3.

Start the calculation using 8 points:

$$n = 8 \quad (128)$$

Repeat the following computations until the desired accuracy is obtained.

Calculate the integration intervals:

$$\Delta_n = \frac{h_2 - h_1}{n} \quad (129)$$

$$g = 0.57735026 \cdot 91896 \cdot \Delta_n \quad (130)$$

$$y = g_1 + \frac{\Delta_n - g}{2} \quad (131)$$

$$GN_2 = \frac{\Delta_n}{2} \sum_{i=0}^{n-1} [N(y + i\Delta_n) + N(y + i\Delta_n + g)] \quad (132)$$

Double the number of points:

$$n = 2n \quad (133)$$

and define

$$GN_1 = GN_2 \quad (134)$$

repeating steps from (129) to (132) it is now possible to compare the two values obtained to see if the required accuracy is achieved: if

$$|GN_1 - GN_2| > \varepsilon |GN_1| \quad (135)$$

then continue increasing the number of points using (133), redefine GN_1 using (134) and repeat again steps from (129) to (132).

When the test (135) fails, the required accuracy has been reached, and the value of the integral is obtained by:

$$TEC = \left(GN_2 + \frac{GN_2 - GN_1}{15} \right) \times 10^{-13} \quad (136)$$

3.4.2 Slant TEC calculation

To compute the electron density at a point P along the slant ray-path defined by the points P_1 and P_2 the following specific geometrical configuration is considered.

3.4.2.1 Geometrical configuration

To simplify the formulation we assume that if α is an angle in (degrees), $\tilde{\alpha}$ is the same angle in (rad):

$$\tilde{\alpha} = \alpha * DR \quad (137)$$

3.4.2.1.1 Zenith angle computation

Figure 1 indicates the geometry involved in the computation of the zenith angle ζ at P_1 .

Calculate:

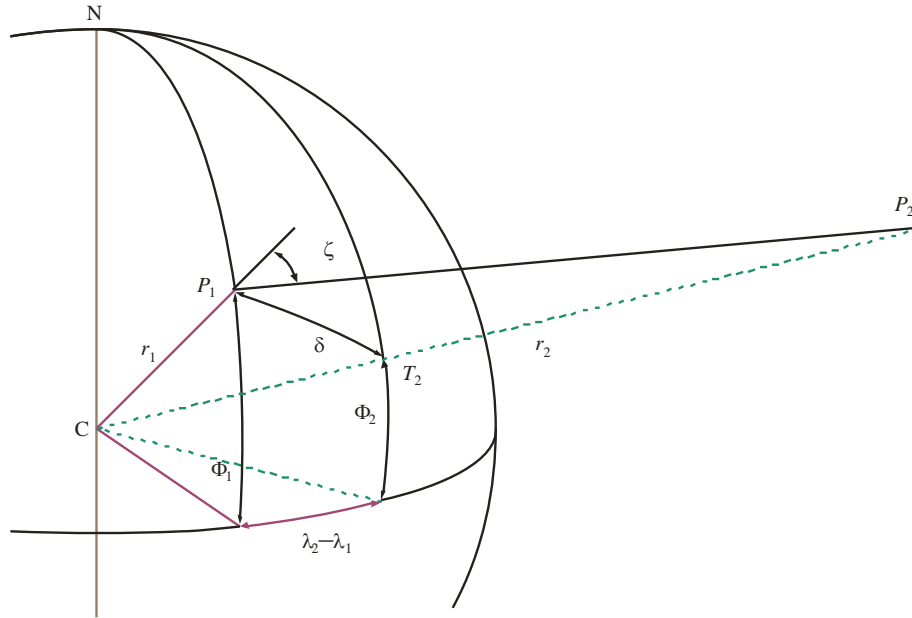
$$\cos \tilde{\delta} = \sin \tilde{\varphi}_1 \sin \tilde{\varphi}_2 + \cos \tilde{\varphi}_1 \cos \tilde{\varphi}_2 \cos (\tilde{\lambda}_2 - \tilde{\lambda}_1) \quad (138)$$

$$\sin \tilde{\delta} = \sqrt{1 - \cos^2 \tilde{\delta}} \quad (139)$$

$$\tilde{\zeta} = \text{atan2} \left(\sin \tilde{\delta}, \cos \tilde{\delta} - \frac{r_1}{r_2} \right) \quad (140)$$

being δ the Earth angle on the great circle connecting the receiver (P_1) and the satellite (P_2). The symbol $\text{atan2}(y,x)$ indicates the function that computes the arctangent of y/x with a range of $(-\pi, \pi]$.

FIGURE 1
Geometry of zenith angle computation



Report P.2297-01

3.4.2.1.2 Ray-perigee computation

Figure 2 indicates the geometry involved in the computation of the coordinates of the ray-perigee P_p : ray-perigee radius r_p (km), ray-perigee latitude φ_p (degrees) and ray-perigee longitude λ_p (degrees).

Calculate r_p :

$$r_p = r_1 \sin \tilde{\zeta} \quad (141)$$

Calculate φ_p :

if $|\varphi_1 - 90^\circ| < 10^{-10}$ use

$$\varphi_p = \begin{cases} \zeta & \text{if } \varphi_1 > 0 \\ -\zeta & \text{if } \varphi_1 < 0 \end{cases} \quad (142)$$

otherwise use

$$\sin \tilde{\sigma} = \frac{\sin(\tilde{\lambda}_2 - \tilde{\lambda}_1) \cos \tilde{\varphi}_2}{\sin \tilde{\delta}} \quad (143)$$

$$\cos \tilde{\sigma} = \frac{\sin \tilde{\varphi}_2 - \cos \tilde{\delta} \sin \tilde{\varphi}_1}{\sin \tilde{\delta} \cos \tilde{\varphi}_1} \quad (144)$$

$$\tilde{\delta}_p = \frac{\pi}{2} - \tilde{\zeta} \quad (145)$$

$$\sin \tilde{\varphi}_p = \sin \tilde{\varphi}_1 \cos \tilde{\delta}_p - \cos \tilde{\varphi}_1 \sin \tilde{\delta}_p \cos \tilde{\sigma} \quad (146)$$

$$\cos \tilde{\varphi}_p = \sqrt{1 - \sin^2 \tilde{\varphi}_p} \quad (147)$$

$$\tilde{\varphi}_p = \text{atan2}(\sin \tilde{\varphi}_p, \cos \tilde{\varphi}_p) \quad (148)$$

Calculate λ_p :

if $|\varphi_1 - 90^\circ| < 10^{-10}$ use

$$\varphi_p = \begin{cases} \zeta & \text{if } \varphi_1 > 0 \\ -\zeta & \text{if } \varphi_1 < 0 \end{cases} \quad (149)$$

otherwise use

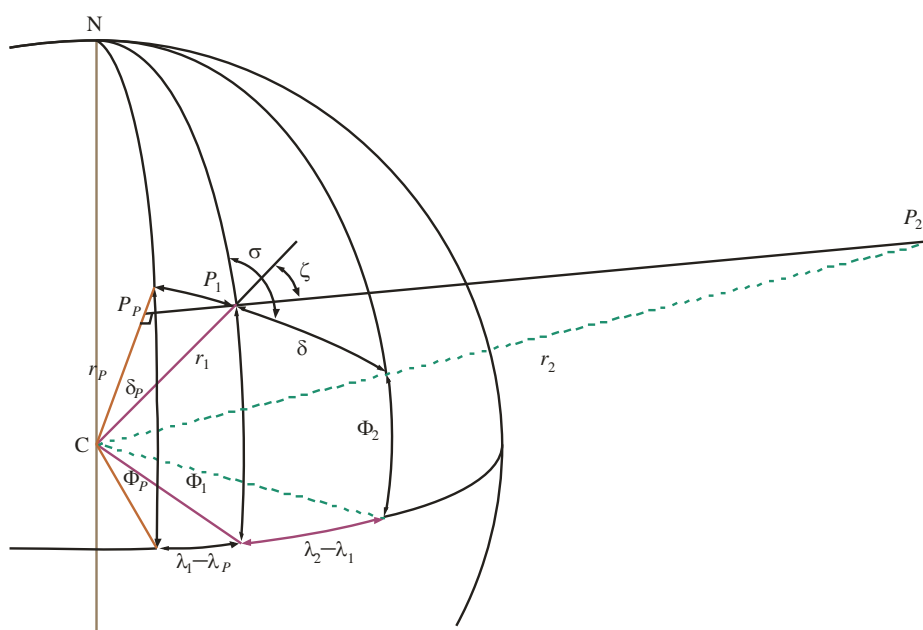
$$\sin(\tilde{\lambda}_1 - \tilde{\lambda}_p) = -\frac{\sin\tilde{\sigma}\sin\tilde{\delta}_p}{\cos\tilde{\varphi}_p} \quad (150)$$

$$\cos(\tilde{\lambda}_1 - \tilde{\lambda}_p) = \frac{\cos\tilde{\delta}_p - \sin\tilde{\varphi}_1\sin\tilde{\varphi}_p}{\cos\tilde{\varphi}_1\cos\tilde{\varphi}_p} \quad (151)$$

$$\lambda_p = [\text{atan2}(\sin(\tilde{\lambda}_1 - \tilde{\lambda}_p), \cos(\tilde{\lambda}_1 - \tilde{\lambda}_p)) + \tilde{\lambda}_1] * RD \quad (152)$$

being σ the azimuth of P_2 seen from P_1 and δ_p the Earth angle between P_1 and the ray-perigee P_p .

FIGURE 2
Geometry of ray-perigee computation



Report P2297-02

3.4.2.1.3 Great circle properties

Compute the great circle angle ψ from ray-perigee to satellite:

if $|\varphi_p| - 90 < 10^{-10}$ use

$$\Psi = |\varphi_2 - \varphi_p| \quad (153)$$

otherwise use

$$\cos\tilde{\Psi} = \sin\tilde{\varphi}_p\sin\tilde{\varphi}_2 + \cos\tilde{\varphi}_p\cos\tilde{\varphi}_2\cos(\tilde{\lambda}_2 - \tilde{\lambda}_p) \quad (154)$$

$$\sin\tilde{\Psi} = \sqrt{1 - \cos^2\tilde{\Psi}} \quad (155)$$

$$\tilde{\Psi} = \text{atan2}(\sin\tilde{\Psi}, \cos\tilde{\Psi}) \quad (156)$$

Compute sine and cosine of azimuth σ of satellite as seen from ray-perigee P_p :

if $|\varphi_p| - 90 < 10^{-10}$ use

$$\sin \tilde{\sigma}_p = 0 \quad (157)$$

$$\cos \tilde{\sigma}_p = \begin{cases} -1 & \text{if } \varphi_p > 0 \\ 1 & \text{if } \varphi_p < 0 \end{cases} \quad (158)$$

otherwise use

$$\sin \tilde{\sigma}_p = -\frac{\cos \tilde{\varphi}_2 \sin(\tilde{\lambda}_2 - \tilde{\lambda}_p)}{\sin \tilde{\Psi}} \quad (159)$$

$$\cos \tilde{\sigma}_p = -\frac{\sin \tilde{\varphi}_2 - \sin \tilde{\varphi}_p \cos \tilde{\Psi}}{\cos \tilde{\varphi}_p \sin \tilde{\Psi}} \quad (160)$$

3.4.2.2 Integration endpoints

Indicating with s_1 and s_2 the distances of P_1 and P_2 respectively from the ray perigee compute:

$$s_1 = \sqrt{r_1^2 - r_p^2} \quad (161)$$

$$s_2 = \sqrt{r_2^2 - r_p^2} \quad (162)$$

3.4.2.3 Coordinates along the integration path: $c(h_s, \varphi_s, \lambda_s)$

Being s (km) the distance of a point P from the ray perigee P_p , $(r_p, \varphi_p, \lambda_p)$ the ray perigee coordinates and $\sin \sigma_p$, $\cos \sigma_p$ the sine and cosine of the azimuth of the satellite as seen from the ray perigee, the coordinates of the point P are calculated by the function c as follows.

Inputs:

Distance s (km), ray-perigee coordinates $(r_p, \varphi_p, \lambda_p)$, sine and cosine of azimuth of satellite as seen from ray perigee $\sin \sigma_p$, $\cos \sigma_p$.

Outputs:

Coordinates of point P : h_s (km), φ_s (degrees), λ_s (degrees)

To compute the geocentric coordinates of any point P (having distance s from the ray perigee P_p) along the integration path, the following formulae have to be applied:

Calculate h_s :

$$h_s = \sqrt{s^2 - r_p^2} - R_E \quad (163)$$

being R_E the Earth mean radius.

Calculate great circle parameters:

$$\tan \tilde{\delta}_s = \frac{s}{r_p} \quad (164)$$

$$\cos \tilde{\delta}_s = \frac{1}{\sqrt{1 + \tan^2 \tilde{\delta}_s}} \quad (165)$$

$$\sin \delta_s = \tan \tilde{\delta}_s \cos \tilde{\delta}_s \quad (166)$$

Calculate φ_s :

$$\sin\tilde{\varphi}_s = \sin\tilde{\varphi}_p \cos\tilde{\delta}_s + \cos\tilde{\varphi}_p \sin\tilde{\delta}_s \cos\tilde{\sigma}_p \quad (167)$$

$$\cos\tilde{\varphi}_s = \sqrt{1 - \sin^2\tilde{\varphi}_s} \quad (168)$$

$$\tilde{\varphi}_s = \text{atan2}(\sin\tilde{\varphi}_s, \cos\tilde{\varphi}_s) * RD \quad (169)$$

Calculate λ_s :

$$\sin(\tilde{\lambda}_s - \tilde{\lambda}_p) = \sin\tilde{\delta}_s \sin\tilde{\sigma}_p \cos\tilde{\varphi}_p \quad (170)$$

$$\cos(\tilde{\lambda}_s - \tilde{\lambda}_p) = \cos\tilde{\delta}_s - \sin\tilde{\varphi}_p \sin\tilde{\varphi}_s \quad (171)$$

$$\lambda_s = \left[\text{atan2}(\sin(\tilde{\lambda}_s - \tilde{\lambda}_p), \cos(\tilde{\lambda}_s - \tilde{\lambda}_p)) + \tilde{\lambda}_p \right] * RD \quad (172)$$

3.4.2.4 Slant TEC numerical integration

To compute slant TEC along a ray-path defined by its perigee coordinates, direction and end-point, a numerical integration algorithm is used. In NeQuick Gauss integration is used and is described in the following.

Inputs:

- h_1 , height of point P_1 (km)
- φ_1 , latitude of point P_1 (degrees)
- λ_1 , longitude of point P_1 (degrees)
- h_2 , height of point P_2 (km)
- φ_2 , latitude of point P_2 (degrees)
- λ_2 , longitude of point P_2 (degrees)

Output:

Slant TEC (10^{15}m^{-2})

One possible numerical algorithm for slant TEC calculation is the following.

In the case of integration from ground to satellite ($h_1 < 1000$ km and $h_2 > 2000$ km) it is convenient to divide the integration path in three parts defining intermediate points s_a, s_b :

$$s_a = \sqrt{(R_E + 1000)^2 - r_p^2} \quad (173)$$

$$s_b = \sqrt{(R_E + 2000)^2 - r_p^2} \quad (174)$$

We have that $(R_E + 1000)^2 = 54334589.44$ and $(R_E + 2000)^2 = 70076989.44$.

The slant TEC becomes therefore:

$$TEC = \int_{s_1}^{s_a} N(s) ds + \int_{s_a}^{s_b} N(s) ds + \int_{s_b}^{s_2} N(s) ds \quad (175)$$

To compute each integral the algorithm described in § 3.4.2.5 can be used as:

$$\int_{s_1}^{s_2} N(s) ds = GN(g_1, g_2, \varepsilon, r_p, \sin\tilde{\varphi}_p, \cos\tilde{\varphi}_p, \sin\tilde{\sigma}_p, \cos\tilde{\sigma}_p, \lambda_p) \quad (176)$$

where the parameter ε indicates the integration accuracy. Here we assume:

- $\varepsilon = 0.001$ for the integration between s_1 and s_a
- $\varepsilon = 0.01$ for the integrations between s_a and s_b and between s_b and s_2

3.4.2.5 Gauss algorithm

Inputs:

- distances from the ray perigee of the first integration endpoint: g_1 (km)
- distances from the ray perigee of the second integration endpoint: g_2 (km)
- Integration accuracy ε
- Ray-perigee parameters: r_p (km), $\sin\tilde{\varphi}_p, \cos\tilde{\varphi}_p, \sin\tilde{\sigma}_p, \cos\tilde{\sigma}_p, \tilde{\lambda}_p$ (degrees)

Output:

TEC [TECu]

To be able to compute NeQuick electron density, in all the following computations it is necessary to calculate the coordinates of the point P along the ray-path using the algorithm illustrated in § 3.4.2.3.

$$(h(s), \varphi(s), \lambda(s)) = c(s, \sin\tilde{\varphi}_p, \cos\tilde{\varphi}_p, \sin\tilde{\sigma}_p, \cos\tilde{\sigma}_p, \tilde{\lambda}_p) \quad (177)$$

Start the calculation using 8 points:

$$n = 8 \quad (178)$$

Repeat the following computations until the desired precision is obtained.

Calculate the integration intervals:

$$\Delta n = \frac{g_2 - g_1}{n} \quad (179)$$

$$g = 0.5773502691896 \cdot \Delta n \quad (180)$$

$$y = g_1 + \frac{\Delta n - g}{2} \quad (181)$$

$$GN_2 = \frac{\Delta n}{2} \sum_{i=0}^{n-1} [f(y + i\Delta n) + f(y + i\Delta n + g)] \quad (182)$$

Double the number of points:

$$n = 2n \quad (183)$$

and define

$$GN_1 = GN_2 \quad (184)$$

repeating steps from (178) to (181) it is now possible to compare the two values obtained to see if the required accuracy is achieved: if

$$|GN_1 - GN_2| > \varepsilon |GN_1| \quad (185)$$

then continue increasing the number of points (183), redefine GN_1 (184) and repeat again steps from (178) to (182).

When the test (185) fails, the required accuracy has been reached, and the value of the integral is obtained by:

$$TEC = \left(GN_2 + \frac{GN_2 - GN_1}{15} \right) \times 10^{-13} \quad (186)$$

3.5 Changes introduced in NeQuick2

The changes introduced in NeQuick 2.1 with respect to the first version of the model are summarized.

The most important modifications introduced are related to the bottomside electron density profile representation and to the shape parameters of the topside ionosphere.

3.5.1 Bottomside modification

The F1 layer formulation has been reformulated [Leitinger *et al.*, 2005, RD2] to avoid the occurrence of the anomalous behaviour of the model reported at heights in the E and F1 layer of the ionosphere.

As listed in § 3.2.4, here we recall the new parameters:

$$hmF1 = \frac{hmE + hmF2}{2} \quad (187)$$

$$foF1 = \begin{cases} 0 & \text{if } foE < 2 \\ 1.4foE & \text{if } foE \geq 2 \text{ and } 1.4foE \leq 0.85foF2 \\ 0.85 \cdot 1.4foE & \text{if } 1.4foE > 0.85foF2 \end{cases} \quad (188)$$

$$B1_{top} = 0.3(hmF2 - hmF1) \quad (189)$$

$$B1_{bot} = 0.5(hmF1 - hmE) \quad (190)$$

$$BE_{top} = \max(0.5(hmF1 - hmE), 7) \quad (191)$$

foE , $foF1$ and $foF2$ are given in (MHz); hmE , $hmF1$ and $hmF2$ are given in (km).

3.5.2 Topside modification

The topside of the F2 layer of the ionosphere is implemented using a semi-Epstein layer representation. The electron density as function of height $N(h)$ in the topside is represented using a height dependent thickness parameter H_0 [RD3]:

$$N(h) = \frac{4NmF2}{(1 + \exp(z))^2} \exp(z) \quad (192)$$

$$z = \frac{h - hmF2}{H_0 \left[1 + \frac{rg(h - hmF2)}{rH_0 + g(h - hmF2)} \right]} \quad (193)$$

in which the constant parameters $r = 100$ and $g = 0.125$ are used. NeQuick 2.1 includes a simplification of the topside thickness parameter H_0 , using a single empirical relation to represent its correlation to the F2 bottomside thickness parameter $B2_{bot}$ [Nava *et al.*, 2008 RD1]:

$$H_0 = k B2_{bot} \quad (194)$$

$$k = 3.22 - 0.0538foF2 - 0.00664hmF2 + 0.113 \frac{hmF2}{B2_{bot}} + 0.00257R_{12} \quad (195)$$

with a value of 1 imposed on k as a lower limit.

3.5.3 Modip map

To get the magnetic coordinates needed by the model for computing the F2 layer peak and F1 layer height the NeQuick ITU-R (version 1) used a map of dip-latitude (diplats.asc). It was necessary to

compute both Modip and Dip at the location of interest. The change in the formulation of the F1 layer in the NeQuick 2.1 now requires only the computation of the Modip.

NeQuick 2.1 model uses a grid of Modip values contained in the file **modip.asc**. To compute the Modip value in a point at latitude ϕ and longitude λ , a third order interpolation is applied as it is explained in § 3.3.3.1. The Modip map included in the package of version 2.1 has been generated with the *magfit* subroutine. The *magfit* subroutine is patterned after the Fortran subroutine in the ITS propagation package, 2006, called *iongrid*, provided by ESA and available at ITU-R in support of Recommendation ITU-R P.1239. It calculates the magnetic dip angle and the gyrofrequency for the given reflection height and location. This calculation is described in § 2 of Recommendation ITU-R P.1239-3 (02-2012).

3.5.4 Other package and source code modifications

The set of CCIR coefficients that have been used in previous versions of the model have been replaced by the set of ITU-R coefficients provided in the *iongrid* program (software provided by ESA and available at ITU-R in support of Recommendation ITU-R P.1239).

From the point of view of FORTRAN programming, version 2 of NeQuick includes various improvements. In particular to avoid the use of the ENTRY statement, new subroutines have been included: *prepNeQ* and *NeNeQ*.

Version 2.1 corrects some formal bugs of earlier NeQuick versions in the management of modip maps. Some computational improvements have also been introduced.

3.6 References

- [RD1] Nava, B., Coisson, P., Radicella, S.M., “A new version of the NeQuick ionosphere electron density model”, *J.of Atmospheric and Solar-Terrestrial Physics*, Iss. 70, 1856-1862, 2008.
- [RD2] Leitinger, R., Zhang, ML, Radicella, S/M., “An improved bottomside for the ionospheric electron density model NeQuick”, *Annals of Geophysics*, 48(3), p. 525-534, 2005.
- [RD3] Coisson, P., Radicella, S.M, Leitinger, R., Nava, B., “Topside electron density in IRI and NeQuick: features and limitations”, *Adv. Space Research.*, 37 (5), p. 937-942, 2006.
- [RD4] Rawer K., “*Propagation of decameter waves (HF-band)*”, in B. Landmark (Ed), *Meteorological and astronomical influences on radio wave propagation*, New York Academic Press, p. 221-250, 1963.

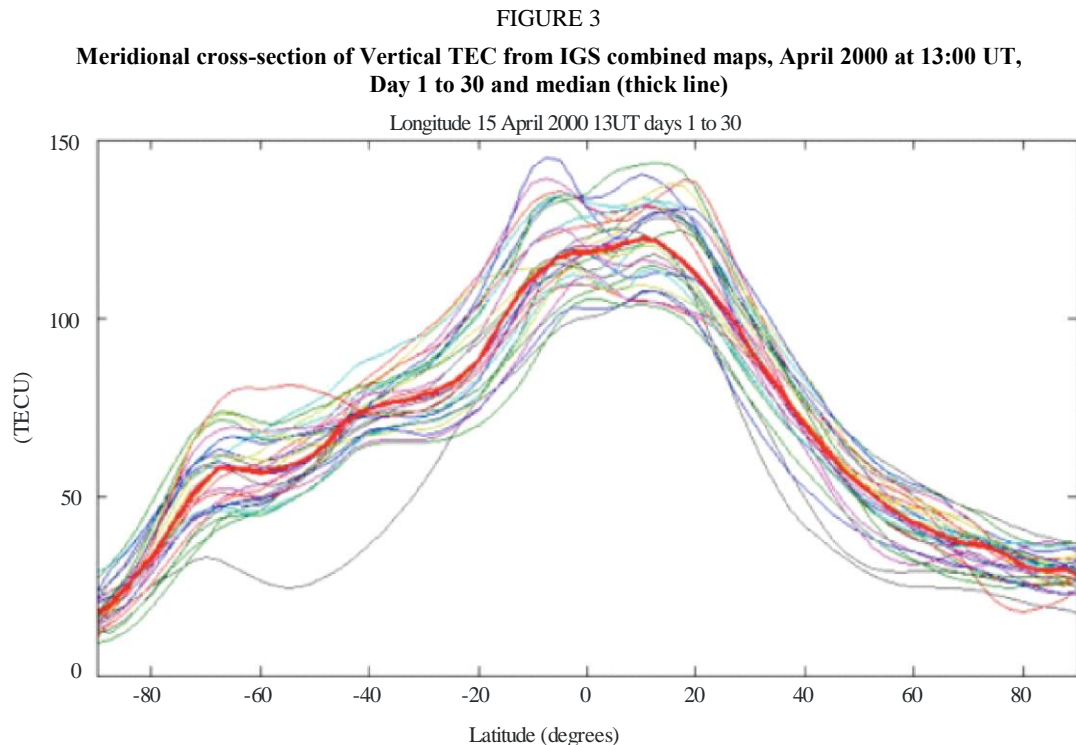
4 Vertical Total Electron Content maps

A set of grid point maps of Vertical Total Electron Content (VTEC) representative of various levels of solar activity are considered of interest for model verification or preliminary assessment of various trans-ionospheric propagation effects such as Faraday rotation, propagation delay, refraction, angle of arrival variation among others. They may be of interest for evaluation of HF propagation. Those maps are available from the Radiocommunication Bureau.

A *de facto* standard widely used by various scientific communities is proposed for the format of the provided VTEC maps. Such format is the IONEX (IONosphere map EXchange) format, see details in: <http://igsceb.jpl.nasa.gov/igsceb/data/format/ionex1.pdf>.

The International GNSS Service (IGS, <http://igsceb.jpl.nasa.gov/components/prods.html>) routinely generates Global Ionospheric Maps (GIMs) in IONEX format on a grid resolution of $2^h \times 5^\circ \times 2.5^\circ$ in UT, longitude and latitude for one day GIMs are routinely generated by four processing centres using dual-frequency GPS observations on a large network of permanent reference stations around the globe, and a final product is obtained by combining the maps from all four processing centres.

Even if monthly median or mean maps together with its inter-quartile range or its standard deviation are provided, the next question is whether they are sufficiently representative of the climatology of the ionosphere. An example of the day-to-day variability and median for 30 days in April 2000 is presented in Fig. 3. In such an example, it is observed that the median curve does not clearly show the very variable equatorial anomaly crests seen in a number of individual days. Another question is related to the symmetry and skewness of the daily values. Examples of the problems of mean/median values and variability are further discussed in the attached presentation.



Report P.2297-03

While the problem of the selection of what can be considered representative is not solved, it is still considered of practical use to incorporate in ITU-R databanks a set of monthly mean maps derived from observations in an accepted grid format, as examples, always remarking the limitations of the averaging and the variability of the ionosphere.

The following test cases, have been derived:

- Three year related to three types solar activity:
 - Solar maximum (2002)
 - Solar minimum (2009)
 - Solar intermediate activity (2005)
- Four sets of 31 days corresponding to different annual seasons, they are derived as 15 days plus and minus the following days:
 - Day of year 79 (Northern hemisphere spring equinox)
 - Day of year 171 (Northern hemisphere summer solstice)
 - Day of year 265 (Northern hemisphere autumn equinox)
 - Day of year 350 (Northern hemisphere winter solstice)

IONEX format supports the inclusion of the VTEC and its standard deviation error. In the VTEC values, the mean value for each grid point over the 31 days has been extracted, and in the standard deviation error, the standard deviation for the 31 days is given.

A set of figures showing the VTEC map and its standard deviation for the three solar activity cases and the month around the Northern hemisphere spring equinox are presented in Fig. 4 as examples of absolute values and variability.

In the future, in order to incorporate information about the range of variability observed around mean values, in addition to the mean maps and its standard deviation, it is suggested to incorporate three daily maps based on certain criteria such as:

- The daily map which minimizes in all points and hours the root mean square error to the mean value.
- The daily map with maximum positive bias (difference between daily map and mean map for all points and hours).
- The daily map with maximum negative bias (difference between daily map and mean map for all points and hours).

FIGURE 4

Mean (left) and standard deviation (right) of VTEC daily maps for a month around the Northern hemisphere spring equinox for low (top), intermediate (middle) and high (bottom) solar activity at 14:00 UT (15:00 UT for high solar activity)

